2015-01-XXXX

Ice Particle Analysis of the Honeywell ALF502 Engine Booster

Author, co-author (Do NOT enter this information. It will be pulled from participant tab in MyTechZone)
Affiliation (Do NOT enter this information. It will be pulled from participant tab in MyTechZone)

Abstract

A flow and ice particle trajectory analysis was performed for the booster of the Honeywell ALF502 engine. The analysis focused on two closely related conditions one of which produced an icing event and another which did not during testing of the ALF502 engine in the Propulsion Systems Lab (PSL) at NASA Glenn Research Center. The flow analysis was generated using the NASA Glenn GlennHT flow solver and the particle analysis was generated using the NASA Glenn LEWICE3D v3.63 ice accretion software. The inflow conditions for the two conditions were similar with the main differences being that the condition that produced the icing event was 6.8 K colder than the non-icing event case and the inflow ice water content (IWC) for the non-icing event case was 50% less than for the icing event case. The particle analysis, which considered sublimation, evaporation and phase change, was generated for a 5 micron ice particle with a sticky impact model and for a 24 micron median volume diameter (MVD), 7 bin ice particle distribution with a supercooled large droplet (SLD) splash model used to simulate ice particle breakup. The results from the analysis showed that the amount of impingement for the components were similar for the same particle size and impact model for the icing and non-icing event conditions. This was attributed to the similar aerodynamic conditions in the booster for the two cases. The particle temperature and melt fraction were higher at the same location and particle size for the non-icing event than for the icing event case due to the higher incoming inflow temperature for the non-event case. The 5 micron ice particle case produced higher impact temperatures and higher melt fractions on the components downstream of the fan than the 24 micron MVD case because the average particle size generated by the particle breakup was larger than 5 microns which yielded less warming and melting. The analysis also showed that the melt fraction and wet bulb temperature icing criterion developed during tests in the Research Altitude Test Facility (RATFac) at the National Research Council (NRC) of Canada were useful in predicting icing events in the ALF502 engine. The development of an ice particle impact model which includes the effects of particle breakup, phase change, and surface state is necessary to further improve the prediction of ice particle transport with phase change through turbomachinery.

Introduction

A large amount of research is currently being conducted to quantify, model and simulate the High Ice Water Content (HIWC) threat [1,2]. The HIWC environment, which contains large ice crystals (> 100 microns) in large concentrations (> 2 g/m^3) at high altitudes (~40,000ft), has been responsible for over 150 incidents including rollbacks and in one case a dead stick landing. The current research includes flight testing, instrument development, ground based facility development and testing and modeling of the ice accretion process in turbo-machinery.

Recently a set of HIWC tests on the Honeywell ALF502 engine were conducted in the newly completed Ice Crystal Engine Test Chamber at the Propulsion Systems Laboratory (PSL) at NASA Glenn Research Center [3]. The tests were able to repeat icing events from flight tests of the engine. The data from these tests is being used to develop and verify computational models with varying levels of fidelity. One topic of interest is determining the conditions that produce icing events and those that do not.

Of particular interest from the recent tests are a pair of closely related test points one of which produced an icing event while the other did not. To further understand the difference between these two conditions a high fidelity flow and icing analysis of the ALF502 low pressure compressor was conducted using the NASA Glenn GlennHT flow solver [4] and the NASA Glenn LEWICE3D ice accretion software [5]. These tools use a 3D, steady mixing plane approach to analyze flow and icing in turbomachinery.

Numerical Method

Grid and Flow Calculations

The GridPro grid generation software was used to develop the three-dimensional grids for the geometry [6] and the GlennHT flow solver [4] was used to generate the flow solutions for the analysis. The GlennHT code is a three-dimensional, finite volume based, Reynolds Averaged Navier-Stokes flow solver. The code computes flow on complex propulsion system configurations using multi-block body fitted grids. The method employs a “mixing-plane” procedure to pass boundary condition data between grid blocks for the steady state flow analysis of turbomachinery. The code supports parallel computing and supports several turbulence models.

Particle Transport Calculations

The LEWICE3D V3.63 grid based icing tool [5,7], which incorporates droplet trajectory, heat transfer and ice shape calculation into a single computer program, was used for the particle transport analysis. This program has several features which allow the analysis of turbomachinery subject to HIWC or SLD environments. These features include a particle splash and bounce algorithm, a geometry

handling scheme which allows complex mirroring, transformation and relative motion of input grid blocks and an algorithm which calculates zone to zone collection efficiencies using a mixing plane approach.

Results

The ALF502 analysis included the calculation of flow and ice particle transport properties. The particle analysis results are presented for a 5 micron particle using a sticky impact model and a 24 micron MVD, 7 bin distribution using an SLD splash model to simulate ice particle breakup. The particle analysis was carried out for two conditions one of which generated an icing event and the other which did not (PSL test point DP0443 and DP0256 respectively). The inflow conditions for the two conditions were similar with the main differences being that the condition that produced the icing event (DP0443) was 6.8 K colder than the non-icing event case (DP0256) and the inflow ice water content (IWC) for the non-icing event case was 50% less than for the icing event case.

The grid and surface model used for the flow and particle analysis is shown in Figures 1-2. The grid contained 33 structured, abutted grid blocks with a total of 1,596,897 nodes. Steady, inviscid flow solutions were generated for DP0256 and DP0443 test conditions. Figure 3 depicts the elements of interest for the compressor. The flow analysis for the DP0256 and DP0433 cases are documented in a companion paper[8].

The LEWICE3D ice particle analysis required several cloud input conditions and modeling parameters. The ice particle analysis assumed an inflow relative humidity of 100% and a particle concentration (IWC) of 2.0 g/m^3 for case DP0443 and 1.0 g/m^3 for case DP0256. The ice particles were assumed to be completely frozen and at the ambient temperature of the surrounding air at the inflow boundary. Two particle conditions were simulated in the analysis for each flow condition. A 5 micron particle size with a sticky impact model was chosen because it has been successful in predicting icing risk in simpler, lower fidelity analysis where it was used to represent the ice particles resulting from the particle breakup in the fan. A 24 micron MVD, 7 bin particle distribution was chosen to match the cloud generated by the PSL spray system. An SLD splash model was chosen for the 24 micron MVD distribution to simulate the ice particle breakup because a model was not available and it was thought that the breakup characteristics of an ice particle were similar to that of a similarly sized water droplet. Although the SLD splash model generates more impingement on a surface than an ice particle impact model due to the stickier nature of liquid water versus ice it is useful because it can give an indication of the location and state of the impacting particles which is useful for assessing regions which are at risk for icing. The ice particle calculations were made from the inflow boundary through the compressor and out the compressor exit boundary.

It is worthwhile to report the definitions and equations used for the particle analysis. These include collection efficiency or impingement efficiency (β), average collection efficiency (β_{ave}), impingement rate (IR), and scoop factor (SF). Impingement efficiency is a non-dimensional measure of the mass flux for a surface and is dependent upon the amount of convergence or dispersion of particles in a flow and the orientation of the surface relative to the particle paths. An impingement efficiency of one means the surface particle flux rate is equal to the free stream particle flux rate. A value less than one means the surface particle flux rate is less than the free stream particle flux rate and a value greater than one means that the surface particle flux rate is greater than the free stream level. The average collection efficiency is defined as

$$\beta_{avg} = \frac{\sum_{n=1}^{n=N} \beta_n \times A_n}{A_{wetted}} \quad (1)$$

Where, N, is the number of surface elements with nonzero impingement and β_n, A_n are the collection efficiency and area of surface element, n, respectively. The wetted area of the element is the sum of the area of the elements which have non-zero impingement for which we have the equation;

$$A_{wetted} = \sum_{n=1}^{n=N} A_n \quad (2)$$

The impingement rate for a surface is defined as:

$$IR = \beta_{avg} \times LWC_\infty \times V_\infty \times A_{wetted} \quad (3)$$

Where, LWC_∞, is the free stream liquid water content and, V_∞, is the free stream speed. The free stream catch fraction or scoop factor (SF) is defined as the ratio of the mass impinging on a component divided by the mass available in the free stream for an area equal to the area bounded by the highlight of the inlet lip. The scoop factor is then;

$$SF = \frac{IR}{IR_\infty} \quad (4)$$

The free stream impingement rate, IR_∞, is defined as the rate at which the particles pass through an area traced out by the highlight of the inlet lip (A_∞) traveling at the free stream speed (V_∞) with an average collection efficiency of 1 and an LWC matching that of the free stream (LWC_∞). The average collection efficiency for a surface is then:

$$\beta_{avg} = \frac{IR \times A_\infty}{IR_\infty \times A_{wetted}} = SF \times \frac{A_\infty}{A_{wetted}} \quad (5)$$

The collection efficiency results for case DP0256 and case DP0443 for both particle sizes are shown in Figure 4. The results show that the collection efficiency on the spinner and fan are larger for the 24 micron MVD, SLD cases than for the 5 micron cases due to the larger inertia of the larger particles. The collection efficiency on the components downstream of the fan are smaller for the larger particles. The reason for the smaller collection efficiency for the larger particle cases is threefold. First, the fan removed more mass for the larger particles making less mass available for the downstream components. This can be seen in Tables 1-4 and Figure 5 where we can see that the scoop factors are much greater for the larger particles. Second, the larger particles are less able to negotiate the flow into the inner core due to the flow curvature. This can be seen in the Figure 6 which shows axial mass flux for particles through the compressor. Thirdly, the reduction in collection efficiency on the components downstream of the fan is due in part to the reduction in average particle size from the particle breakup for the larger SLD splash model cases. Figure 7 shows that the average particle size for the cases decreases as the particles pass through the compressor. At

the fan exit the average particle size for the 24 micron MVD, SLD splash model cases is approximately 18 microns. At the inflow to IGV #1 the average particle size is approximately 9 microns.

The average particle size for all cases decreased through the low pressure compressor. For the 5 micron cases, which did not involve a breakup model, the reduction in particle size was small and was the result of sublimation and evaporation. The average particle size change for the 24 micron MVD, SLD splash model cases, which were predominantly due to particle breakup, were much larger than for the 5 micron cases. From Figure 8 we can see the mass loss due to evaporation and sublimation was greater for the warmer cases (DP0256) and was largest for the 24 micron MVD, SLD splash model case (28%). The 24 MVD micron, DP0256 SLD splash model breakup case produced smaller particles which were subject to more sublimation and evaporation than the 5 micron DP0256 case. This is because particle sublimation and evaporation increases with increased temperature and with the increased surface area of the smaller sized particle cloud. The particle breakup resulted in an approximate reduction of 33% in the average particle size at the inflow to IGV #1 and approximately 25% at the exit of the transition duct (Fig. 7). The majority of the reduction in particle size due to breakup occurs in the fan and the entrance to the inner core. This is because the SLD splash model breakup model generates less ejected mass and larger ejected particles as the impacting particle size is reduced. It is also due in part to the lower impingement rates and impact speeds for the smaller particles which more readily adapt to changes in the flow about the engine components. The particle distributions at various axial locations in the compressor are shown for the SLD splash model cases in Figure 9. From the figure we can see that there are some differences in the particle distributions for the intermediate stages but that the distributions at the fan outflow and at the duct exit are similar for both the DP0256 and DP0443, 24 MVD micron, SLD splash model cases. The particle breakup results in a reduction in the average particle size along with a reduction in the minimum and maximum particle size in the distribution. For both cases the maximum particle size in the distribution was reduced from 67 microns to 12 microns while the minimum particle was reduced to 2 microns from 7 microns.

In general the mass transport properties through the compressor were similar for case DP0256 and case DP0443 for the same particle size. This is due to the similarity in the flow conditions for the two cases. The mass transport properties of the particles are predominantly dependent on the flow velocity and density and particle size which can be characterized by the modified inertia parameter. For both flow cases the rotational speed was the same and the inlet pressure, temperature and velocity were similar which yielded a similar flow. The modified inertia parameter for the 5 micron particle was 0.01773 for case DP0256 and 0.01747 for case DP0443. For the 24 micron MVD, SLD splash model cases, the modified inertia parameters at the MVD drop size of the distribution (24 microns) were 0.02181 and 0.02149 for DP0256 and DP0443 respectively.

The average particle impact temperatures for the low pressure compressor are shown in Figure 10. The particle temperature increases as it transits the warming environment of the compressor. In all cases the average particle temperature lags the local static temperature and the lag in temperature increases with increased particle size due to the increased thermal mass of the larger particles. The DP0256 cases produced higher final particle temperatures than those for DP0443 due to the higher inflow temperature. The particle temperature approaches the wet bulb temperature of the flow as the particle becomes fully melted as can be seen in Figure 11 for the 5 micron cases.

The melt fraction results are shown in Figures 12,13. From the figures one can see that there is no appreciable melting for any of the cases until the outflow of rotor #1. The melt fractions are higher for the warmer cases at the same particle size. The average melt fractions at the compressor exit are also higher for the 5 micron mono-disperse cases than for the SLD splash model cases because the average particle size is larger for the SLD splash model cases. The average melt fraction for the DP0443, SLD splash model case was 0.68 while the particles for the other three cases were fully melted at the duct exit. From the contour plots of the melt fraction one can see a large increase in melt fraction below the mid span location for EGV #2 and aft of the trailing edge of the EGV #2 on the outer duct wall. This is due to the impact of much smaller particles which are more readily warmed and melted than the larger particles in the surrounding regions (Fig. 14).

Although the calculated transport data does not produce ice shape predictions it can be examined using icing sensitivity parameters developed previously to better understand the potential for ice growth and significant performance losses in the compressor. Previously researchers have isolated two parameters which are useful in assessing the potential for an icing event [9-12]. These are the melt fraction and the wet bulb temperature. It is known that ice crystal icing requires some amount of water for the ice to adhere and that the wet bulb temperature of the flow be less than several degrees above freezing for the ice to grow. If the particles are 100% ice they bounce or breakup and are ejected from the surface. If the wet bulb temperature is too much above freezing the convective heat load is too high and ice growth cannot be sustained. Tests of several geometries in the NRC RATFac showed that ice build-up was produced for a range of melt fractions of 0.05-0.32 and at wet bulb temperatures below 5.5^{o}C[11]. From Figure 15 we can see that for the warmer DP0256 cases that the range of melting fractions between 0.05-0.32 occurs upstream of EGV #2. The wet bulb temperature is above 278.65 K in this range which would indicate that ice buildup should not occur. For the DP0443 case we have a wet bulb temperature of less than 278.65 K in the region where the melt fraction is between 0.05-0.32 indicating that icing is possible.

Although the average values of particle temperature and melt fractions are useful in assessing relative risk they do not give information as to the location of the icing risk. An examination of the local values of surface temperature, pressure, velocity and particle impact concentration, temperature and melt fraction are required to deduce this. If we look at the particle impact melt fraction and temperature surface contour plots for the DP0443, 24 micron MVD, SLD splash model case (Fig. 10,12) we see that the conditions near the intersection of EGV #2 and the outer duct wall indicate ice accretion based on the above criterion. If we look at the same region for the warmer DP0226, SLD splash model case we see that the melt fraction is too high (> .4) indicating that icing would probably not occur.

The present analysis although useful in understanding the relative effect of particle breakup and phase change falls short as an accurate assessment of the ice particle transport with phase change through booster. A more accurate analysis requires the development of an ice particle impact model which includes the effects of particle breakup, phase change, and surface state.

Conclusions

The GlennHT flow solver and the LEWICE3D icing software were used to analyze the ALF502 low speed compressor for two closely related conditions one of which generated an icing event and one which did not during testing in the PSL engine icing test facility. The main differences between the two cases were the inflow temperature which was 6.8 K cooler for the condition that generated the icing event and the inflow IWC which was 50% lower for the non-icing event case. The collection efficiency results at the same particle size for the two cases were similar due to the similarity in the aerodynamic conditions. The collection efficiency results showed that the collection efficiencies were larger for the larger SLD splash model cases upstream of the splitter lip but smaller for the SLD splash model cases downstream of the splitter lip due to the removal of mass by the fan and spinner, the reduction in particle size caused by impact with the fan and spinner and due to the flow curvature limiting the amount of larger particles transiting into the core. The particle breakup generated a reduction in the average particle size of approximately 33% for the larger SLD splash model cases. The majority of the breakup (25%) occurred in the spinner, fan and splitter lip regions. The thermal analysis showed that the larger particles warmed less and produced less melting than the smaller particles due to their increased thermal mass. The larger SLD splash model cases produced more mass loss than the smaller particle cases because they produced a large amount of smaller particles during impact (< 5 microns) which were more susceptible to sublimation and evaporation. The icing risk criterion developed during the NRC tests for melt fraction (0.05 > melt fraction < .32) and wet bulb temperatures (< 5.5^{o}C) was useful in predicting the icing risk for the ALF502 low pressure compressor for the two test points selected for this analysis. The criterion showed that the icing event case (DP0443) was susceptible to icing in the EGV #2-outer duct intersection region and that the particle melt fractions and temperatures were too high to generate icing for the warmer non-icing event (DP0226). These results show that the GlennHT/LEWICE3D steady, mixing plane approach can be useful for predicting icing risk in turbomachinery. The development of an ice particle impact model which includes the effects of particle breakup, phase change, and surface state is necessary to further improve the utility of these tools in the prediction of ice particle transport with phase change through turbomachinery.

References

1. Mason, J; Strapp, W and Chow, P; "The Ice Particle Threat to Engines in Flight", 44th AIAA Aerospace Sciences Meeting, v4, 2006, pp2445-2465.
2. Mazzawy R.S., Strapp J.W.; "Appendix D – An Interim Icing Envelope; SAE 2007-01-3311; *SAE 2007 Aircraft and Engine Icing International Conference*; Seville, Spain, November 2007.
3. Oliver, M., "Validation Ice Crystal Icing Engine Test in the Propulsion Systems Laboratory at NASA Glenn Research Center," AIAA 2014-2898, 2014.
4. Steinthorsson, E., Liou, M., and Povinelli, L., "Development of an Explicit Multiblock/Multigrid Flow Solver for Viscous Flows in Complex Geometries," AIAA–93–2380 (NASA TM–106356), 1993.
5. Bidwell, C., Potapczuk, M., "Users Manual for the NASA Lewis Three-Dimensional Ice Accretion Code (LEWICE3D)," NASA TM-105974, December 1993.
6. Program Development Corporation., "GridPro GUI Manual Version 1.0," September 24, 2014.
7. Bidwell, C., "A Lagrangian Parcel Based Mixing Plane Method for Calculating Water Based Mixed Phase Particle Flows in Turbo-machinery," DOI 10.1007/s40571-015-0033-z, Journal of Computational Particle Mechanics, February, 2015.
8. Rigby, D., Bidwell, C.,"Three Dimensional Navier-Stokes Simulation of Flow in an Axial Low Pressure Compressor at Engine Icing Operating Conditions", SAE 15ICE-0139, June 2015.
9. Tsao, J., Struk, P., Oliver, M., "Possible Mechanisms for Turbofan Engine Crystal Icing at High Altitude," AIAA 2014-3044, 2014.
10. Jorgenson, P., Veres, J., "Modeling Commercial Turbofan Engine Icing Risk With Ice Crystal Ingestion," AIAA 2013-2679, 2013.
11. Wright, W., Jorgenson, P., Veres, J., "Mixed Phase Modeling in GlennICE with Application to Engine Icing," AIAA 2010-7674, 2010.
12. Currie, T., Fuleki, D., Mahallati, A., "Experimental Studies of Mixed-Phase Sticking Efficiency for Ice Crystal Accretion in Jet Engines," AIAA 2014-3049, 2014.

Nomenclature

A	area, m^2
BETA	collection efficiency
D	ice particle diameter, μm
DIAMAVG	particle diameter, μm
DPMFRAC	particle melt fraction
DPTEMP	particle temperature, K
EGV	exit guide vane
IGV	inlet guide vane
IR	impingement rate, g/s
IWC	ice water content, g/m^3
LWC	liquid water content, g/m^3
MVD	median volume diameter, μm
SF	scoop factor
SLD	supercooled large droplet
V	velocity, m/s
β	impingement efficiency

Appendix

Table 1. Transport statistics for case DP0256, 5 micron mono-disperse, sticky impact.

Element	Impingement Rate (g/s)	Scoop Factor	D_{avg} (μm)	T_{avg} (K)	Melt Fraction$_{avg}$
Inlet Capture	201.162	1.0000	5.00	260.10	0.000
Spinner	0.005	0.0001	4.95	267.70	0.000
Fan Blade	11.001	0.1094	4.99	267.83	0.000
Splitter Lip	0.412	0.0041	4.97	273.15	0.006
IGV #1	2.047	0.0204	4.96	273.15	0.018
Rotor #1	1.205	0.0120	4.93	273.15	0.086
EGV #1	0.528	0.0053	4.91	273.15	0.189
EGV #2	0.905	0.0090	4.86	273.15	0.468
EGV #2+EGV #3+wall	0.168	0.0017	4.88	273.15	0.401
Inner Core Exit	2.606	0.0259	4.58	286.87	1.000

Table 2. Transport statistics for case DP0443, 5 micron mono-disperse, sticky impact.

Element	Impingement Rate (g/s)	Scoop Factor	D_{avg} (μm)	T_{avg} (K)	Melt Fraction$_{avg}$
Inlet Capture	191.528	1.0000	5.00	253.30	0.000
Spinner	0.009	0.0001	4.96	261.62	0.000
Fan Blade	23.872	0.1246	5.01	263.03	0.000
Splitter Lip	0.589	0.0031	5.00	268.75	0.000
IGV #1	4.026	0.0210	4.99	268.10	0.000
Rotor #1	2.558	0.0134	4.97	271.92	0.000
EGV #1	1.099	0.0057	4.96	273.15	0.011
EGV #2	1.869	0.0098	4.93	273.15	0.156
EGV #2+EGV #3+wall	0.357	0.0019	4.94	273.15	0.111
Inner Core Exit	5.397	0.0282	4.69	281.75	1.000

Table 3. Transport statistics for case DP0256, 24 micron MVD, 7 Bin, SLD splash model.

Element	Impingement Rate (g/s)	Scoop Factor	D_{avg} (μm)	T_{avg} (K)	Melt Fraction$_{avg}$
Inlet Capture	201.162	1.0000	24.00	260.10	0.000
Spinner	4.178	0.0415	37.73	264.80	0.000
Fan Blade	35.521	0.3532	22.09	265.39	0.000
Splitter Lip	0.119	0.0012	12.54	271.60	0.000
IGV #1	0.249	0.0025	9.57	273.15	0.007
Rotor #1	0.173	0.0017	9.49	273.15	0.064
EGV #1	0.179	0.0018	11.28	273.15	0.088
EGV #2	0.061	0.0006	6.19	273.15	0.465
EGV #2+EGV #3+wall	0.086	0.0009	12.15	273.15	0.130
Inner Core Exit	0.177	0.0018	5.94	277.54	1.000

Table 4. Transport statistics for case DP0443, 24 micron MVD, 7 bin, SLD splash model.

Element	Impingement Rate (g/s)	Scoop Factor	D_{avg} (μm)	T_{avg} (K)	Melt Fraction$_{avg}$
Inlet Capture	191.528	1.0000	24.00	253.30	0.000
Spinner	8.270	0.0432	37.97	257.86	0.000
Fan Blade	75.016	0.3917	23.07	258.89	0.000
Splitter Lip	0.145	0.0008	11.82	265.02	0.000
IGV #1	0.307	0.0016	9.27	266.03	0.000
Rotor #1	0.208	0.0011	9.33	269.36	0.000
EGV #1	0.195	0.0010	10.07	272.02	0.000
EGV #2	0.080	0.0004	7.06	273.15	0.134
EGV #2+EGV #3+wall	0.062	0.0003	10.98	273.15	0.045
Inner Core Exit	0.211	0.0011	6.84	273.15	0.678

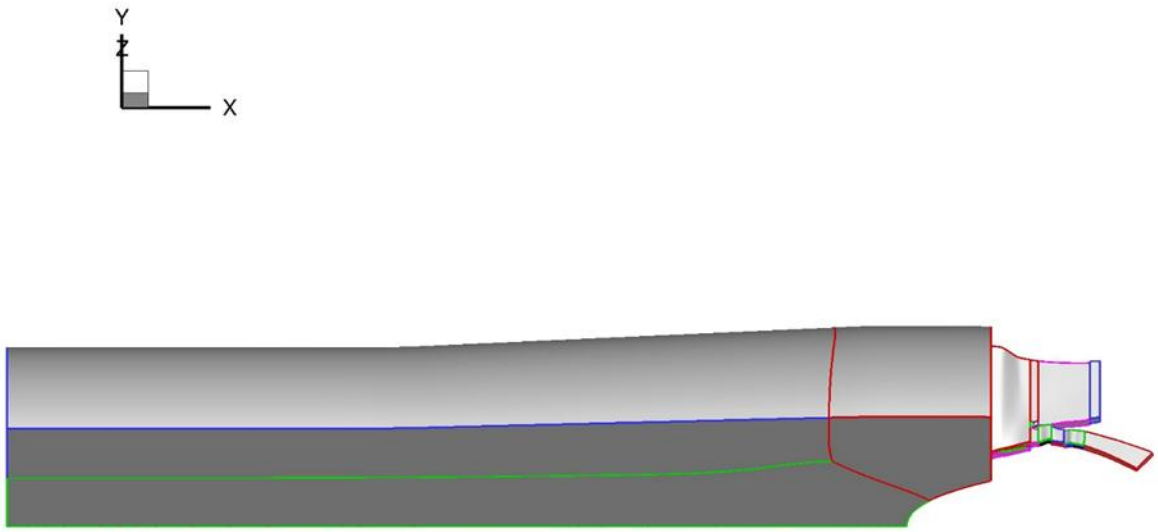

Figure 1. Grid structure.

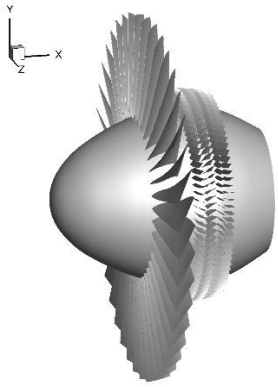

Figure 2. Surface model.

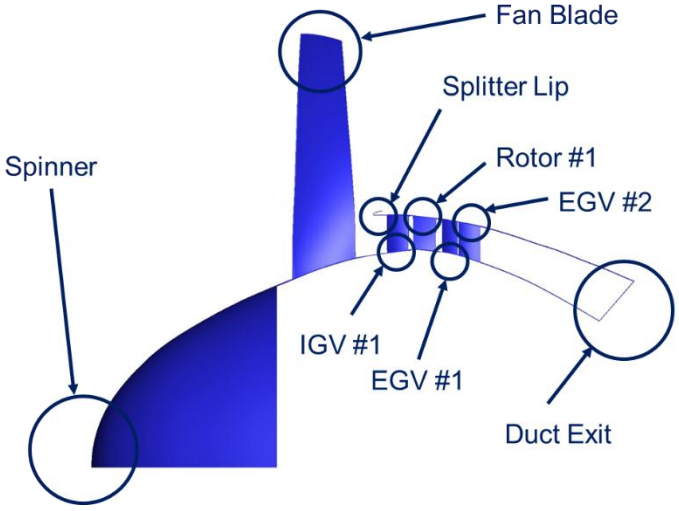

Figure 3. Element description.

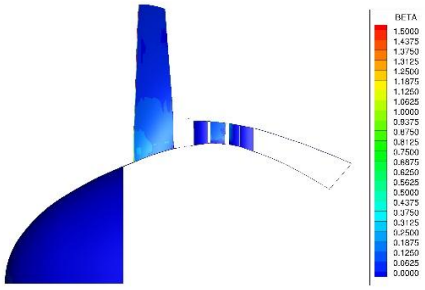

a) DP0256, 5 micron

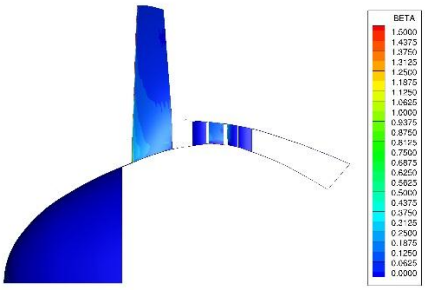

b) DP0443, 5 micron

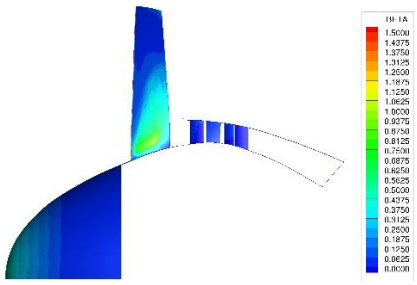

c) DP0256, 24 micron MVD, SLD splash model

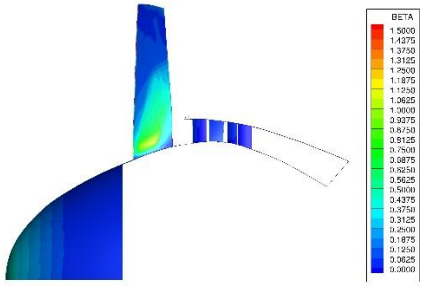

d) DP0443, 24 micron MVD, SLD splash model

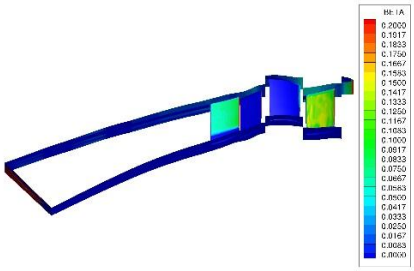

e) DP0256, 5 micron

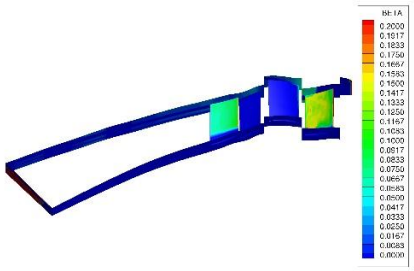

f) DP0443, 5 micron

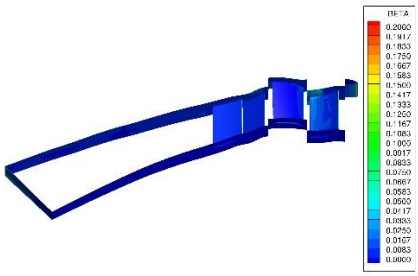

g) DP0256, 24 micron MVD, SLD splash model

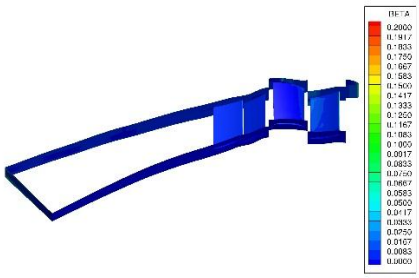

h) DP0443, 24 Micron MVD, SLD splash model

Figure 4. Collection efficiency for booster.

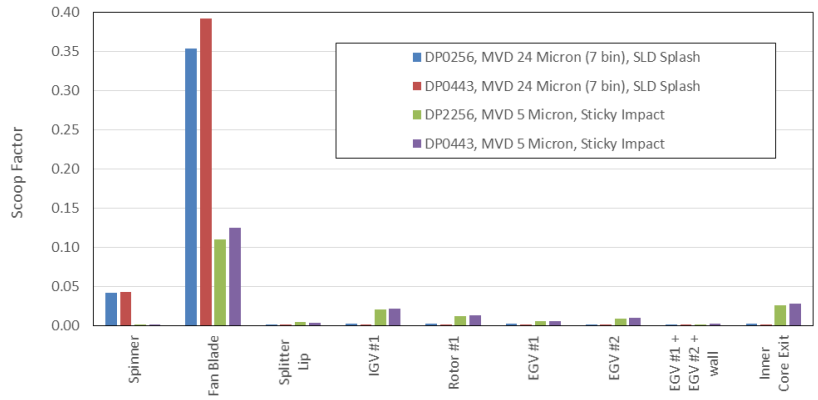

Figure 5. Scoop factor for compressor components.

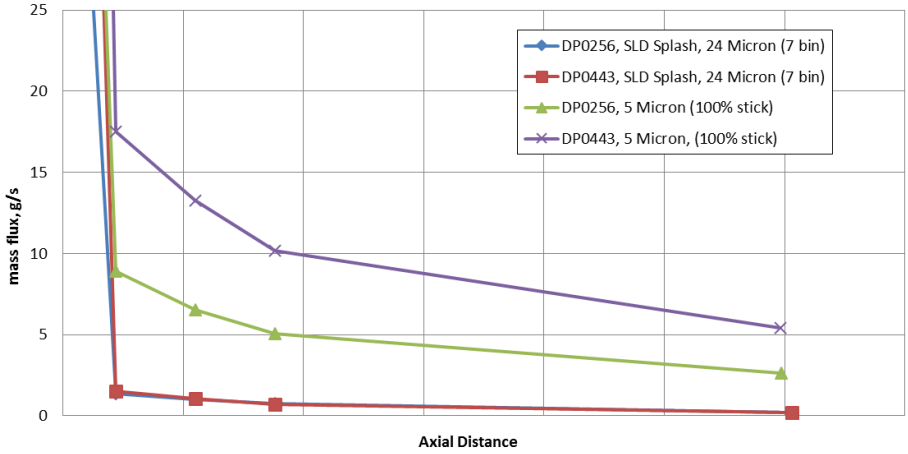

Figure 6. Mass flux rates for the compressor

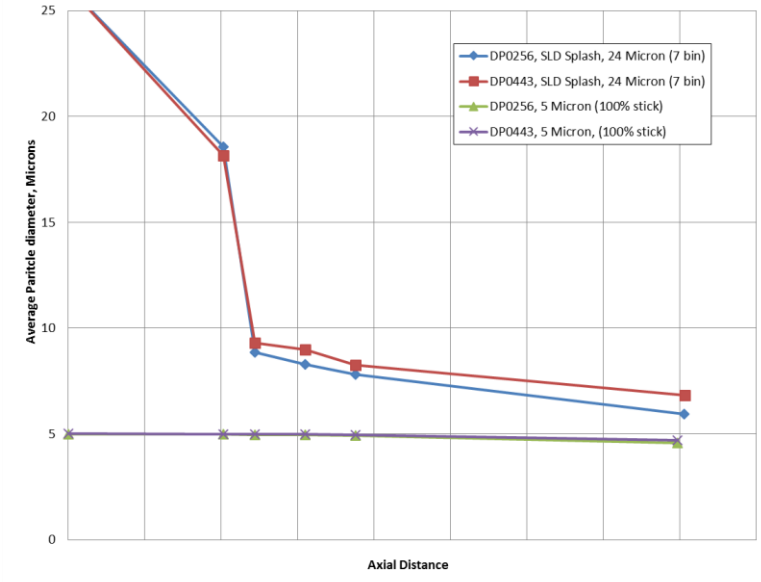

Figure 7. Average particle size for the compressor.

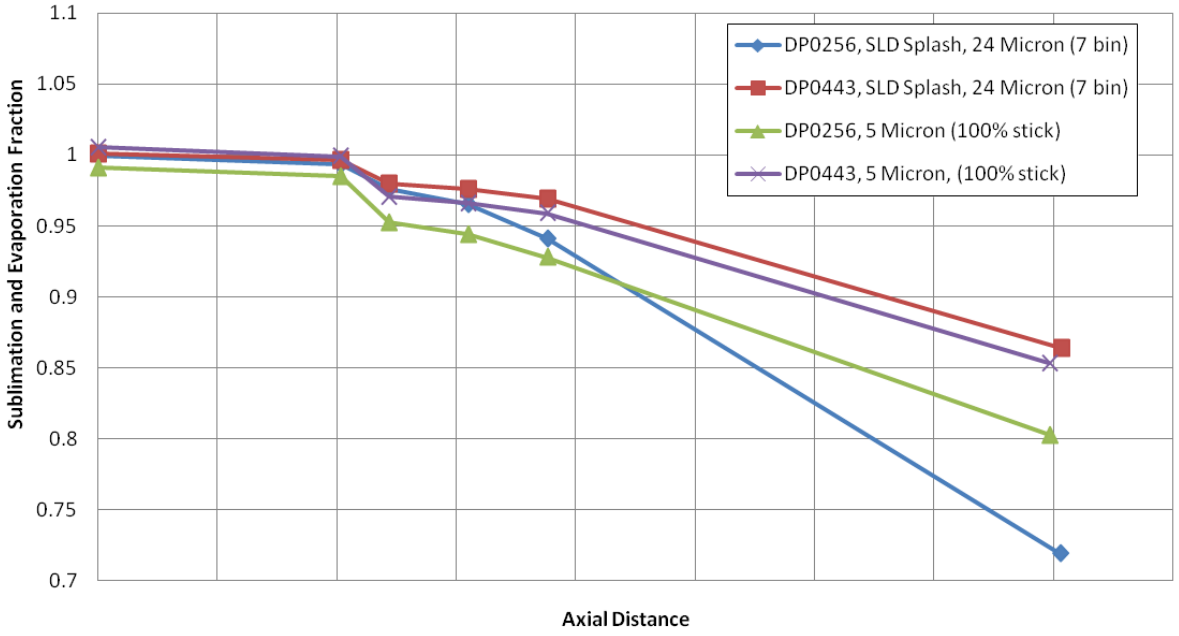

Figure 8. Particle mass loss for the compressor due to sublimation and evaporation.

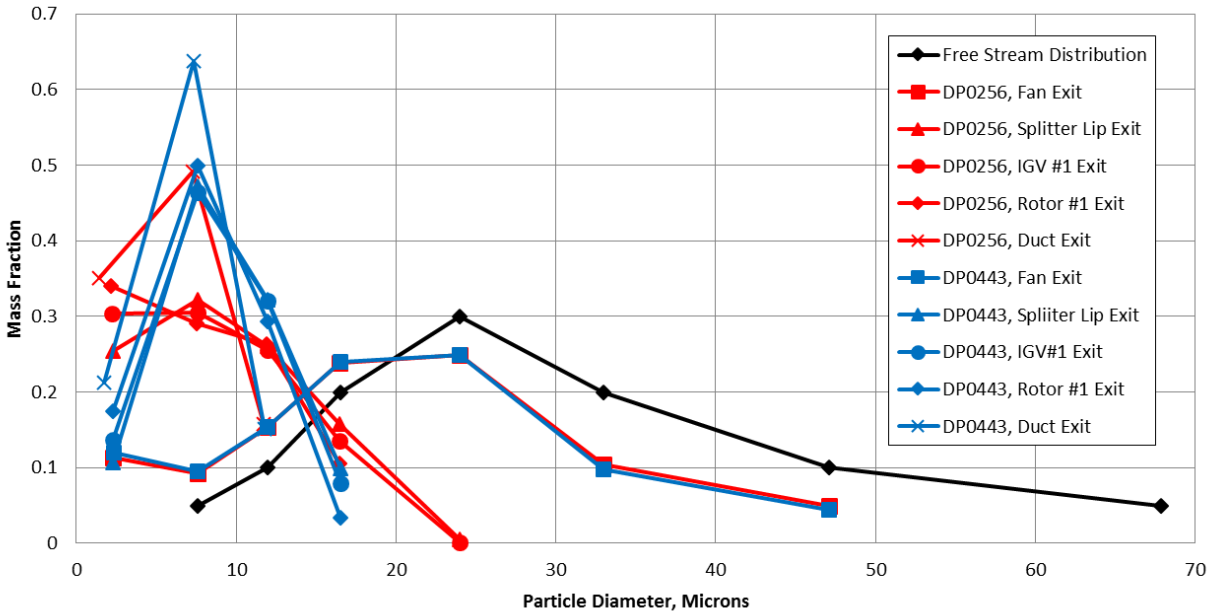

Figure 9. Compressor particle distributions for 24 Micron MVD, SLD splash model cases.

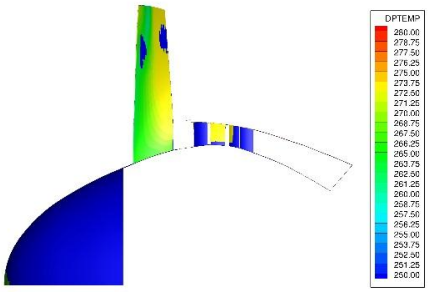

a) DP0256, 5 micron

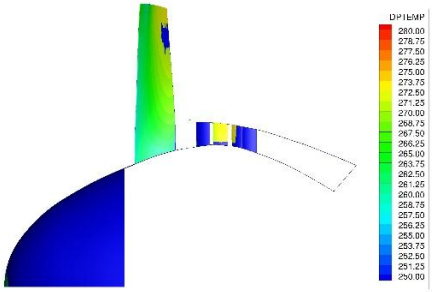

b) DP0443, 5 microns

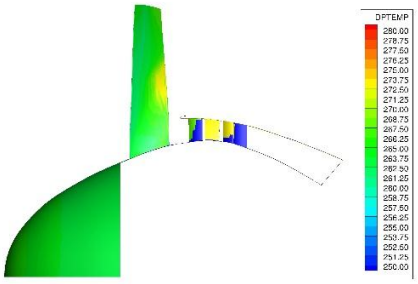

c) DP256, 24 micron MVD, SLD splash model

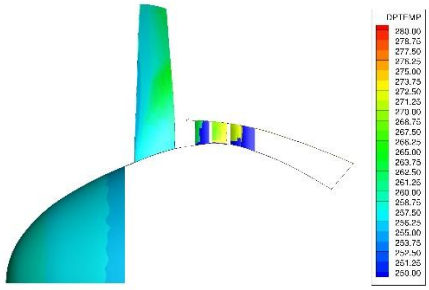

d) DP0443, 24 micron MVD, SLD splash model

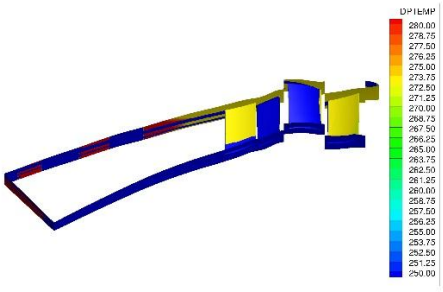

e) DP0256, 5 micron

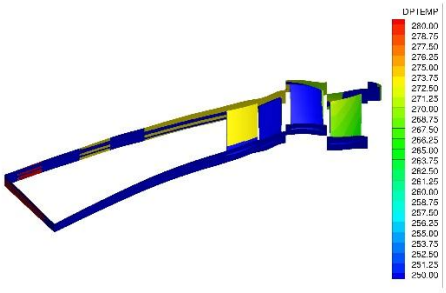

f) DP0443, 5 micron

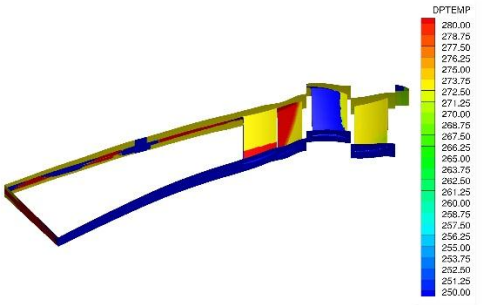

g) DP0256, 24 micron MVD, SLD splash model

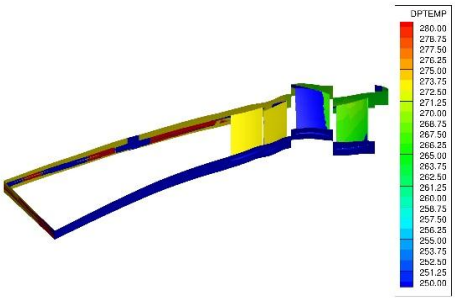

h) DP0443, 24 micron MVD, SLD splash model

Figure 10. Particle impact temperature distributions for compressor.

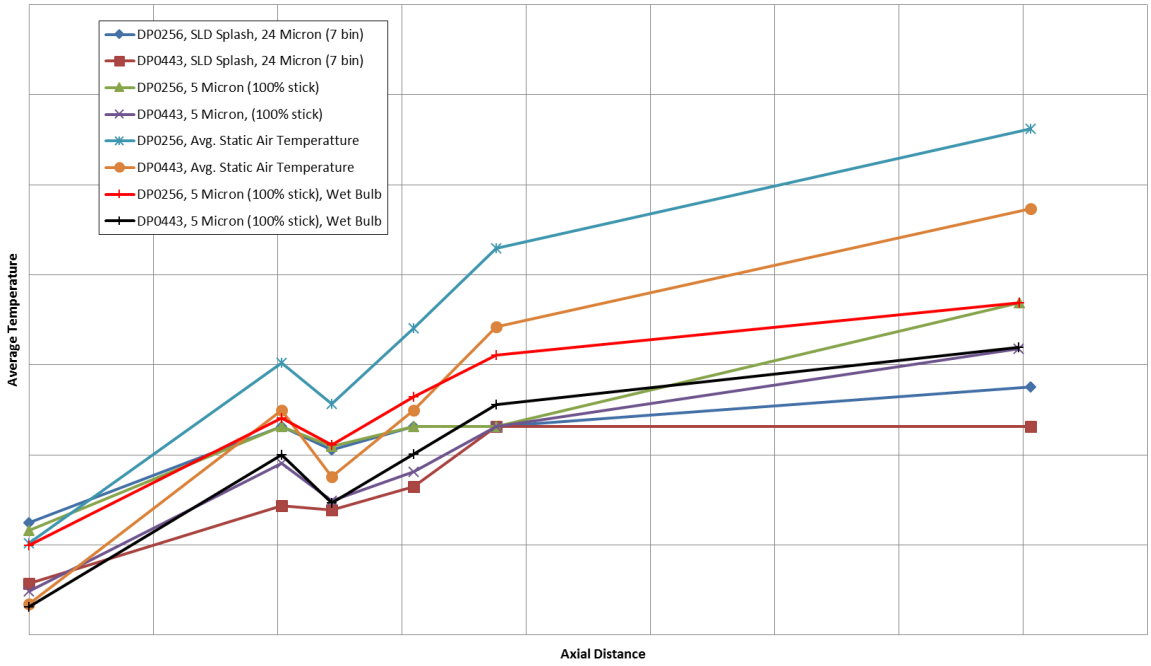

Figure 11. Flow and particle temperatures for compressor.

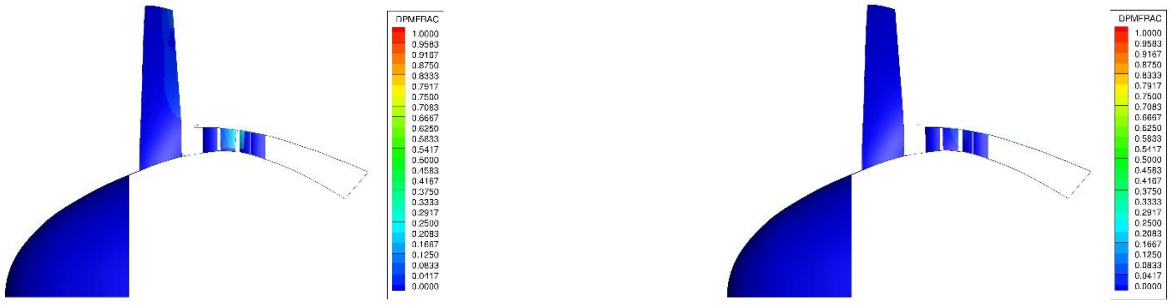

a) DP0256, 5 micron

b) DP0443, 5 micron

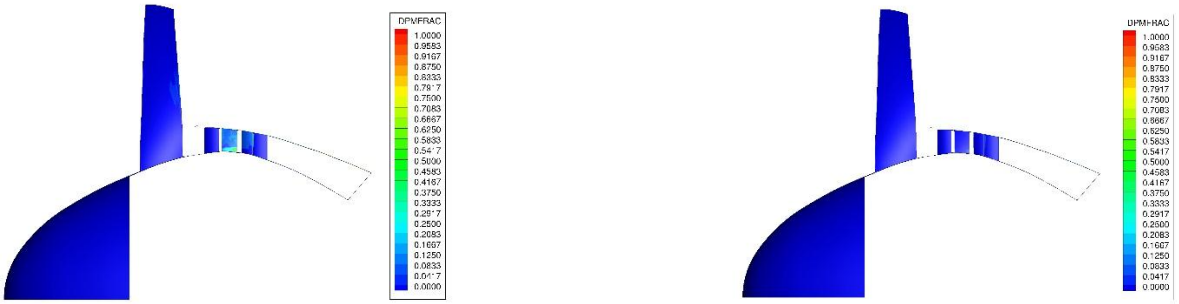

c) DP0256, 24 micron MVD, SLD splash model

d) DP0443, 24 micron MVD, SLD splash model

Figure 12. Particle impact melt fraction distributions for compressor.

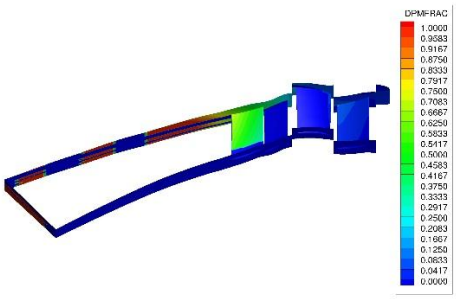

e) DP0256, 5 micron

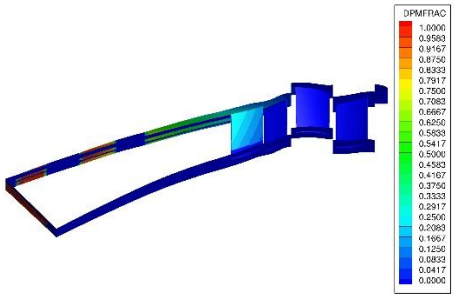

f) DP0443, 5 micron

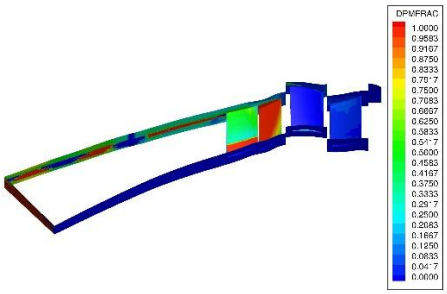

g) DP0256, 24 micron MVD, SLD splash model

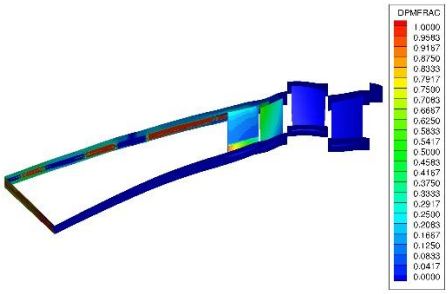

h) DP0443, 24 microns MVD, SLD splash model

Figure 12 concluded. Particle impact melt fraction distributions for compressor.

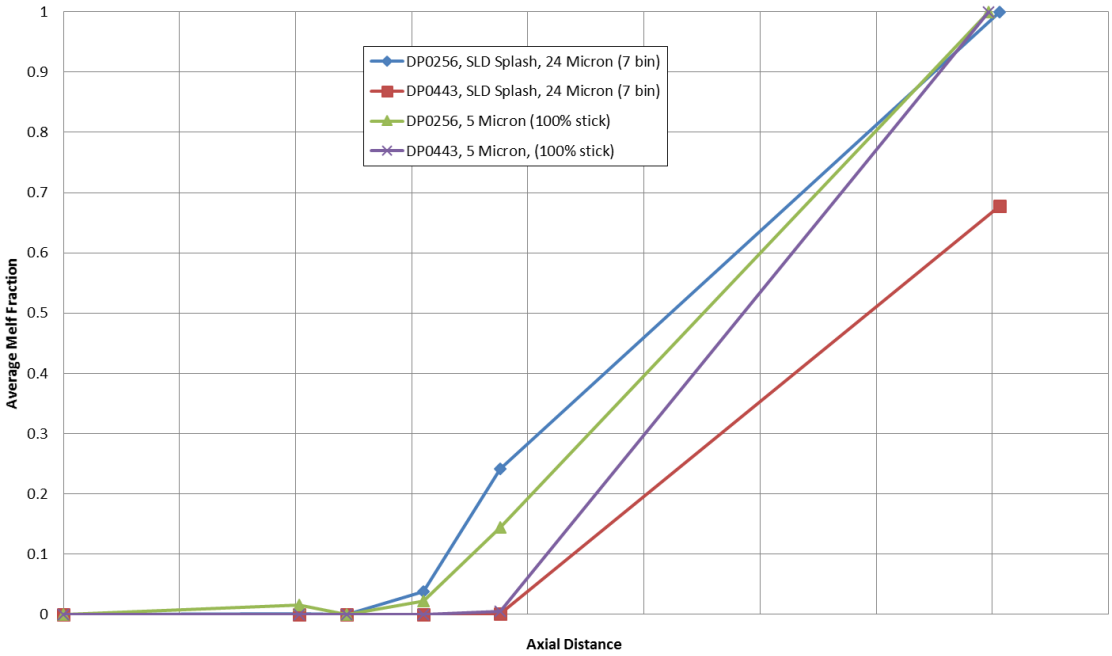

Figure 13. Average particle impact melt fractions for compressor.

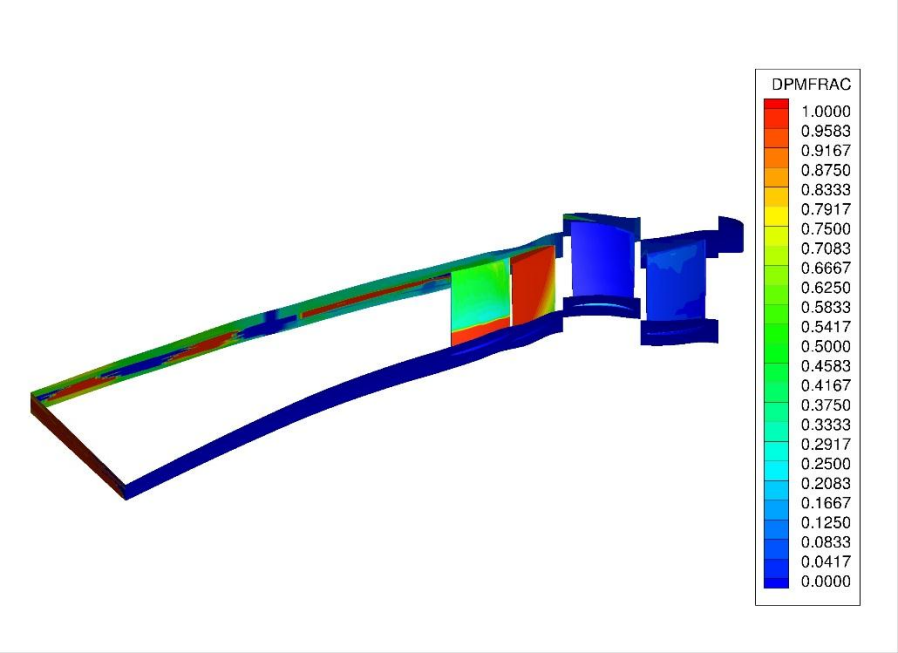

a) Impact particle melt fraction

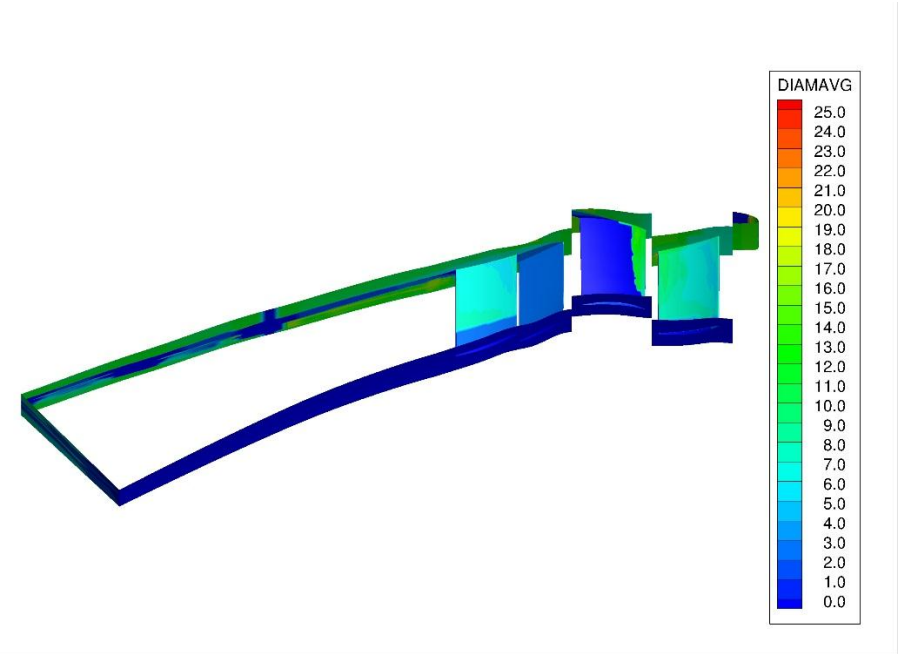

b) Average impact particle diameter

Figure 14. Compressor impact particle distributions for DP0256, 24 micron MVD, SLD splash model.

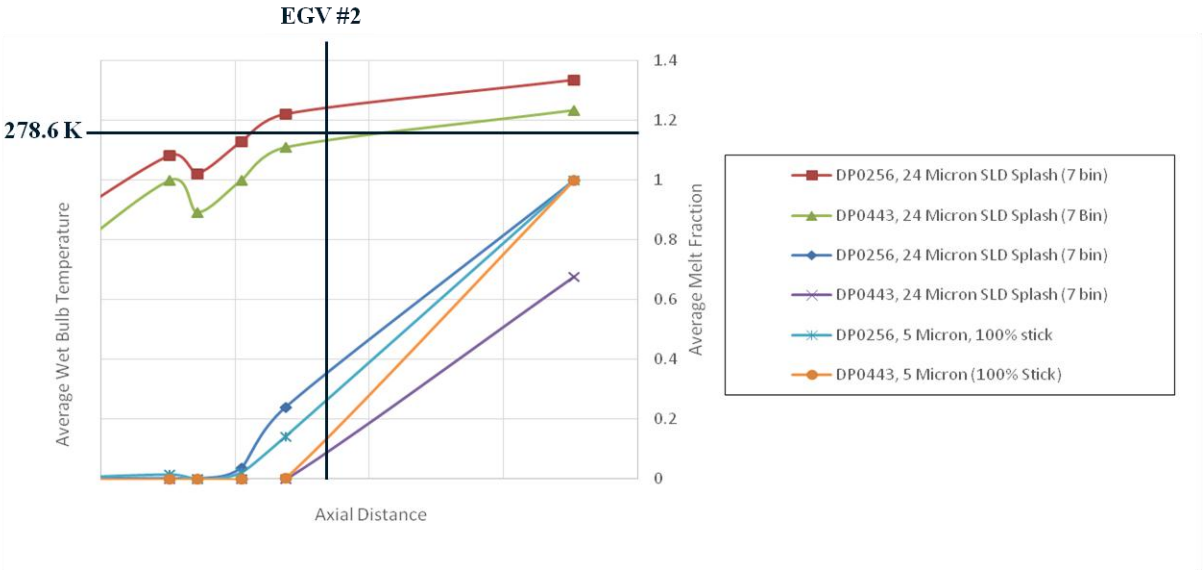

Figure 15. Compressor wet bulb temperature and melt fraction distributions for 24 micron MVD, SLD splash model cases.